

# A nonparametric Bayesian approach to simultaneous subject and cell heterogeneity discovery for single cell RNA-seq data

Qiuyu Wu Xiangyu Luo\*

Institute of Statistics and Big Data, Renmin University of China

## Abstract

The advent of the single cell sequencing era opens new avenues for the personalized treatment. The first but important step is to discover the subject heterogeneity at the single cell resolution. In this article, we address the *two-level-clustering* problem of simultaneous subject subgroup discovery (*subject level*) and cell type detection (*cell level*) based on the scRNA-seq data from multiple subjects. However, the current statistical approaches either cluster cells without considering the subject heterogeneity or group subjects not using the single-cell information. To overcome the challenges and fill the gap between cell clustering and subject grouping, we develop a solid nonparametric Bayesian model SCSC (Subject and Cell clustering for Single-Cell expression data) to achieve subject and cell grouping at the same time. SCSC does not need to prespecify the subject subgroup number or the cell type number, automatically induces subject subgroup structures and matches cell types across subjects, and directly models the scRNA-seq raw count data by deliberately considering the data's dropouts, library sizes, and over-dispersion. A computationally efficient blocked Gibbs sampler is proposed for the posterior inference. The simulation and the application to a multi-subject iPSC scRNA-seq dataset validate the function of SCSC to discover subject and cell heterogeneity.

*Keywords:* High-throughput single-cell genomic data; Nonparametric Bayes; Mixture of mixtures; Nonignorable dropout mechanism; Markov chain Monte Carlo.

---

\*To whom correspondence should be addressed (xiangyuluo@ruc.edu.cn)

# 1 Introduction

The fast advancement in the single cell technology has enabled the expression profiling for thousands of cells simultaneously, resulting in rich accumulations of the single cell RNA-seq (scRNA-seq) data in the public databases, for example, the Gene Expression Omnibus (Edgar et al., 2002), the Human Cell Atlas (Rozenblatt-Rosen et al., 2017). Integrating the scRNA-seq data from multiple subjects gives rise to unprecedented opportunities to analyze and investigate the subject heterogeneity at the single cell resolution. The subject heterogeneity is referred to as the human race subpopulations, the patient disease subtypes, or other differentiable human biological characteristics according to different contexts. Using the disease subtypes as an illustration, previous biological studies have found differences in tumor cell proportions among subtypes of breast cancers (Makki, 2015), lung cancers (Busch et al., 2016) and other diseases. The subtle observations can be captured by the scRNA-seq data but may be missed using the traditional expression data from microarray or bulk RNA-seq, which are the aggregated expression signals from diverse cell types. As a result, there is an urgent need to employ the scRNA-seq data to tease apart the cellular heterogeneity and obtain insights into the subject heterogeneity.

Specifically, we formulate the subject and cell heterogeneity discovery problem as a two-level clustering statistical problem by directly modeling the multi-subject scRNA-seq data, which are demonstrated in Figure 1(a). The Figure 1(b) displays an artificial demonstration of the two-level clustering. At the cell level, the cells having similar expression values are clustered together. At the subject level, the subjects having similar cellular distributions are grouped. Two subjects are said to have the same cellular distributions if they share the cell type proportions and the expression levels for each cell type. In addition, to obtain valid biological results, we need to match the cell types across subjects by considering the effects caused by the subject subgroups (Figure 1(b)). We notice that our two-level clustering problem is different from the bi-clustering (Cheng and Church, 2000; Turner et al., 2005; Prelic et al., 2006) which groups subjects and genes using the aggregated expression data matrix.

However, analyzing the scRNA-seq data suffers from several statistical challenges. First,

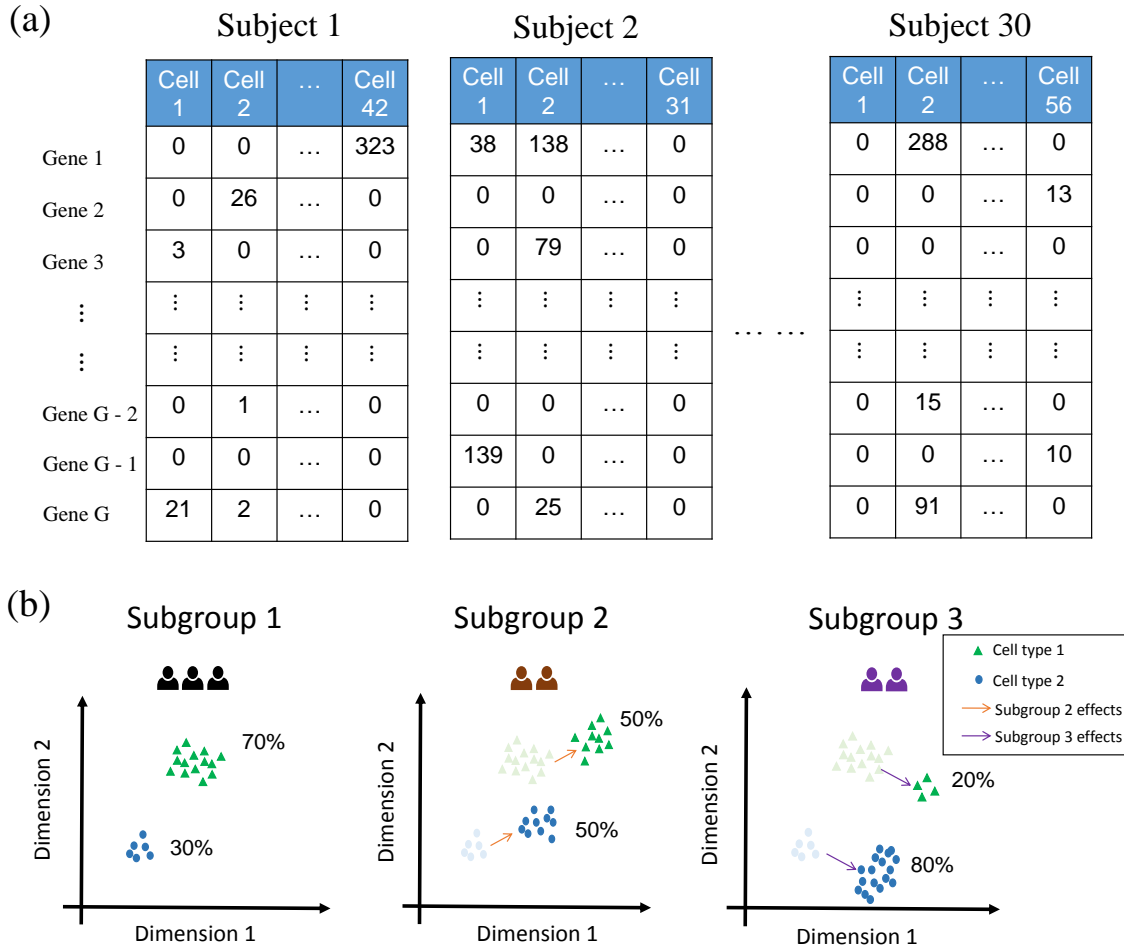


Figure 1: An artificial illustration of the data structure and the study goal. (a) The data structure of the multi-subject scRNA-seq data. One subject corresponds to a count data matrix. In the matrix, each column is a cell and each row is a gene. The gene number  $G$  keeps the same across subjects, while the cell number varies from one subject to another. (b) Based on the count data matrices, our study aims to identify subject subgroups at the subject level and cluster cells at the cell level. In subgroup 1, there are 70% cell type 1 in green triangles and 30% cell type 2 in blue dots. Compared to subgroup 1, the cellular distribution in subgroup 2 can change in two ways, the cell proportions and the cell locations. For a good visualization, only two gene dimensions are illustrated (expression in log scale). The brown and purple arrows represent the subgroup 2 and 3 effects, respectively, when the subgroup 1 is treated as a reference.

the scRNA-seq data are read counts and reveal over-dispersion. The conventional normal or Poisson distribution assumption does not apply to the scRNA-seq data. Second, in contrast to bulk RNA-seq data, the scRNA-seq counts have a relatively large proportion of zeros. This zero-inflation phenomenon, also called dropouts, is mainly caused by a low amount of mRNA molecules in one cell, so the expression levels on some genes are hard to surpass the measurable threshold, thus leading to the zero values. The dropout rate of one cell relies on the corresponding library size and the underlying true expression level of each gene (Jia et al., 2017). Therefore, modeling the dropout events plays a crucial role in correctly analyzing the scRNA-seq data. See Figure 1(a) for a cartoon illustration for the multi-subject scRNA-seq data structure.

There has been a large number of statistical literature working on cell clustering within one subject. They can be classified as three categories: direct clustering, dimension reduction followed by clustering, and imputation followed by clustering. The direct clustering methods model the heterogeneous scRNA-seq data via the latent variable model (Buettner et al., 2015), the hierarchical clustering (Yau et al., 2016), the consensus approach that integrates results from multiple clustering techniques (Kiselev et al., 2017), or the mixture models (Prabhakaran et al., 2016; Sun et al., 2017; Song et al., 2019; Liu et al., 2019). Recently, some fast clustering approaches were developed, which are tractable on ultra-large datasets (Ntranos et al., 2016; Sinha et al., 2018; Lopez et al., 2018). The dimension reduction methods include the classical approaches PCA, tSNE (Der Maaten and Hinton, 2008), as well as approaches specially designed for scRNA-seq, such as the zero-inflated factor analysis (ZIFA) (Pierson and Yau, 2015), ZINB-WaVE (Risso et al., 2018), and UMAP (Becht et al., 2019). Next, clustering is conducted in the low-dimension latent space. The zero-imputation approaches (Lin et al., 2017; Van Dijk et al., 2017; Huang et al., 2018; Zhang and Zhang, 2018) first impute the excess zeros and then carry out clustering on the imputed data. Nevertheless, when applied to the multi-subject scRNA-seq data, all the methods do not consider the subject heterogeneity and ignore the fact that the gene expression levels can change with subjects, thus possibly leading to incorrect cell clustering results.

On the other hand, a plethora of statistical models is proposed to cluster subjects based

on the aggregated expression matrix with genes in row and subjects in column, where the expression vector of one subject can be viewed as the row sums of the subject’s gene-cell expression matrix in Figure 1(a). Pan and Shen (2007) adopted a normal mixture model and developed an  $L_1$ -penalized expectation-maximization algorithm to distinguish subjects and detect differentially expressed (DE) genes. Wang and Zhu (2008) instead used the  $L_\infty$  and hierarchical penalties to refine the clustering results. The sparse K-means proposed by Witten and Tibshirani (2010) simultaneously extracted a few DE genes and grouped subjects by maximizing weighted between-cluster sum-of-squares. Huo et al. (2016) subsequently generalized the sparse K-means to the expression data from multiple studies. Later, Luo and Wei (2019) proposed a more efficient and flexible Bayesian framework to conduct integrative subject clustering. The bi-clustering techniques (Cheng and Church, 2000; Turner et al., 2005; Prelic et al., 2006) achieved subject clustering and feature allocation, where each subject corresponds to a data vector. Therefore, when one subject corresponds to a data matrix as in our case, the subject-clustering methods fail to be applicable.

Moreover, most methods mentioned above require a predetermination of the cluster number and need to try multiple choices, which may be practically difficult and computationally expensive. The nonparametric Bayesian prior—Dirichlet process (DP) (Ferguson, 1973; Sethuraman, 1991)—is well-known for its flexibility of automatically selecting the cluster number in a data-driven manner. However, the DP only addresses one-level clustering, which motivates two extensions—the hierarchical DP (HDP) (Teh et al., 2006) and the nested DP (NDP) (Rodriguez et al., 2008)—that are close to our two-level clustering problem. Unfortunately, using the terms in our context, the HDP assigns a cell mixture distribution to each subject but with different mixture weights, so the subjects cannot form a group structure. Although NDP promotes the subject group structure, subjects in different groups do not share the cell components, which causes difficulty in matching cell types across subjects.

To the best of our knowledge, there is no statistical approach to simultaneously tackle the subject and cell clustering on the multi-subject scRNA-seq data. For the two-level clustering part, we develop a novel nonparametric Bayesian prior that hybridizes the advantages of HDP and NDP, inducing shared components for cells and group structures for subjects. For the data

modeling part, we take advantage of the zero-inflated Poisson-log-normal (ZIPLN) distribution with a Probit dropout mechanism, which accounts for zero-inflation, over-dispersion, and count nature of scRNA-seq data. Integrating the nonparametric Bayesian prior with the ZIPLN distribution arrives at our model SCSC that enables simultaneous subject and cell clustering for the scRNA-seq raw count data and does not require any specification for the subject or cell cluster number in advance. For the posterior inference of SCSC, we design an efficient blocked Gibbs sampler (Ishwaran and James, 2001) based on an approximation model to SCSC. The approximation accuracy is guaranteed theoretically as long as the model truncation numbers and related parameters are appropriately chosen.

We organize our paper as follows. Section 2 presents a brief review of DP and its two extensions, HDP and NDP, which motivates us to propose a hybrid nonparametric Bayesian prior enjoying the strengths of HDP and NDP. In Section 3, we develop the SCSC model that is built upon the hybrid prior and tailored to the scRNA-seq data. An efficient posterior sampling scheme for SCSC is discussed and provided in Section 4, and its application to synthetic data and real world data is illustrated in Section 5. We end our paper with a discussion in Section 6.

## 2 Preliminaries on Nonparametric Priors

Suppose that the scRNA-seq data are collected for  $m$  subjects with subject  $j$  having  $n_j$  sequenced cells in some tissue, and in each cell the expression levels for  $G$  genes are measured. We denote by  $X_{gi}^{(j)}$  the observed read count mapped to gene  $g$  in cell  $i$  for subject  $j$ . All the read counts for subject  $j$  can be wrapped up using a data matrix  $\mathbf{X}^{(j)}$  with  $G$  genes in row and  $n_j$  cells in column. To describe the subject heterogeneity, we assume that subjects can be separated to form several subgroups, where subjects in the same subgroup enjoy similar characteristics and subjects in different subgroups have distinct features. We use  $S^{(j)}$  to represent which subgroup subject  $j$  belongs to. Similarly, the cell heterogeneity is characterized by cell types, and the cell type of cell  $i$  for subject  $j$  is denoted by  $C_i^{(j)}$ . Note that  $\mathbf{X}^{(j)}$ 's are observed but the subject subgroup and cell type indicators need to be estimated.

## 2.1 The Dirichlet Process

The DP (Ferguson, 1973) can be understood as a generalized version of the finite mixture model. For notation simplicity, we temporarily only consider the data on cells from subject 1 and let the gene number  $G$  be one, thus the column vectors  $\mathbf{X}_1^{(1)}, \dots, \mathbf{X}_{n_1}^{(1)}$  of  $\mathbf{X}^{(1)}$  can be simplified to univariate samples  $X_1, \dots, X_{n_1}$  and the cell type indicators  $C_i^{(1)}$ 's to  $C_i$ 's. The finite mixture model allocates each cell to one of  $K$  cell types with a probability to cell type  $k$  being  $\pi_k$ , i.e.,  $Pr(C_i = k) = \pi_k$ , and  $\sum_{k=1}^K \pi_k = 1$ . Given that cell  $i$  is assigned to cell type  $k$ ,  $X_i$  is assumed to be from the distribution  $f(x|\mu_k)$ , where  $f$  is a probability density (or mass) function which will be specified in the next section, and  $\mu_k$  is a parameter describing the cell-type- $k$  effect. Usually, the total cell type number  $K$  is unknown to data analysts, and it is challenging to accurately estimate the value of  $K$ . The DP overcomes the challenge by generalizing  $K$  to infinity and allowing finite non-empty components, hence not requiring a prespecification of  $K$ .

The construction of the DP is realized by the stick-breaking process (Sethuraman, 1991). Imagine that we have a stick with length one and we are going to break this stick into infinite pieces. We first sample a value  $\psi_1$  from the beta distribution  $\text{Beta}(1, \alpha)$  ( $\alpha > 0$ ) and then cut the stick at the place  $\psi_1$  away from the stick's left endpoint. Accordingly, the  $\pi_1$  ( $:= \psi_1$ )-long piece is kept, and we continue to break the remaining stick with length  $1 - \pi_1$ . Once again, we generate a value  $\psi_2$  from  $\text{Beta}(1, \alpha)$ , cut off  $\psi_2$  proportion of the  $1 - \pi_1$ -long stick, and obtain a new piece with length  $\pi_2 := (1 - \pi_1)\psi_2$ . Repeating the breaking procedure on the stick, we have an infinite number of pieces with  $k$ th piece's length  $\pi_k := (1 - \sum_{i=1}^{k-1} \pi_i) \cdot \psi_k$  ( $\psi_k \sim \text{Beta}(1, \alpha)$ ). Each piece  $k$  is further given a mark (parameter)  $\mu_k$  sampled from a distribution  $H$ . In this way, we construct a probability measure,  $P = \sum_{k=1}^{\infty} \pi_k \delta_{\mu_k}$  ( $\delta_{\mu}$  indicates the Dirac measure at  $\mu$ ), with infinite weights  $\{\pi_k\}_{k=1}^{\infty}$  and the support on infinite atoms  $\{\mu_k\}_{k=1}^{\infty}$ . The measure  $P$  is said to be from a DP with the concentration parameter  $\alpha$  and the base distribution  $H$ , written as  $P \sim \text{DP}(\alpha, H)$ . Under  $P$ , each cell  $i$  has the probability  $\pi_k$  to be from cell type  $k$  for any positive integer  $k$  without a constraint  $K$ .

## 2.2 The Hierarchical Dirichlet Process and the Nested Dirichlet Process

The DP is only applicable for one level clustering. When another subject level exists, the HDP (Teh et al., 2006) aims to cluster cells for each subject and is able to match cell types in different subjects. In other words, if the cell type indicators  $C_{i_1}^{(j_1)}$  and  $C_{i_2}^{(j_2)}$  are equal ( $j_1$  may not be  $j_2$ ), then the cell  $i_1$  in subject  $j_1$  and the cell  $i_2$  in subject  $j_2$  must be from the same cell type. Assume  $G^{(j)}$  is the subject- $j$ -specific distribution having a form  $\sum_{k=1}^{\infty} \pi_k^{(j)} \delta_{\mu_k^{(j)}}$ , based on which the cells in subject  $j$  are clustered. To encourage a common support set across  $G^{(j)}$ 's, HDP adopts a hierarchy structure.  $G_0 \sim \text{DP}(\alpha, H)$  at the higher level and  $G^{(j)}$ 's are then i.i.d. generated from  $\text{DP}(\gamma, G_0)$  at the lower level. Since the  $G_0$  from  $\text{DP}(\alpha, H)$  is a discrete distribution and it plays the role of the base distribution in  $\text{DP}(\gamma, G_0)$ , the atoms  $\mu_k^{(j)}$ 's of the support of  $G^{(j)}$  must be consistent with those of  $G_0$ . This characteristic guarantees the shared cell types across  $G^{(j)}$ 's in HDP.

Nevertheless, in HDP, any two subjects have distinct cell distributions due to different weights (cell proportions), i.e.,  $Pr(G^{(j_1)} = G^{(j_2)}) = 0$  if  $j_1 \neq j_2$ , thus no group structure exists among subjects (Figure 2(a)). The NDP (Rodriguez et al., 2008) permits subject grouping while clustering cells. This ability of NDP is achieved by replacing the base measure  $G_0$  in  $\text{DP}(\gamma, G_0)$  with a Dirichlet process  $\text{DP}(\alpha, H)$ , written as  $\text{DP}(\gamma, \text{DP}(\alpha, H))$ . Specifically, if we let  $Q = \text{DP}(\gamma, \text{DP}(\alpha, H))$ ,  $Q$  takes the form of  $\sum_{k=1}^{\infty} \phi_k \delta_{G_k^*}$ , where the atoms of  $Q$  are not numerical values but the distributions  $G_k^*$ 's from  $\text{DP}(\alpha, H)$ . Subsequently,  $G^{(j)}$ 's are i.i.d. sampled from  $Q$  and  $Pr(G^{(j)} = G_k^*) = \phi_k$ . Rodriguez et al. (2008) shows that there is a positive probability that two distributions  $G^{(j_1)}$  and  $G^{(j_2)}$  are identical, thus inducing group structures for  $G^{(j)}$ 's, see Figure 2(b). Despite the simultaneous clustering on subjects and cells enjoyed by NDP, its assumed continuous measure  $H$  leads to totally distinct supports between two subject subgroups, see Figure 2(b). Two subjects' distributions from NDP either share the support atoms and cell proportions or do not have any common atom or cell proportion, hence causing difficulty in cell-type-matching for two different subject subgroups.



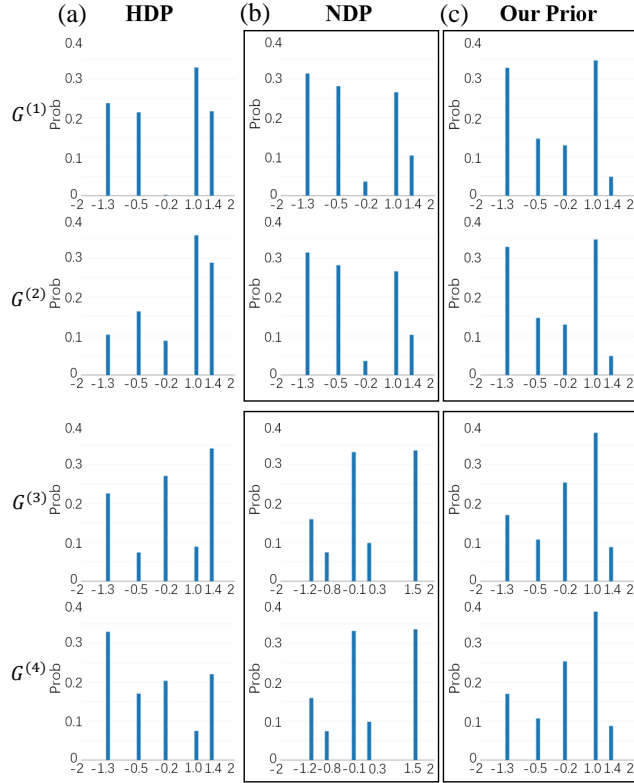


Figure 2: The simple demonstrations of three nonparametric Bayesian priors, HDP, NDP, and our prior. (a) HDP can make subject-specific distributions  $G^{(1)}$ ,  $G^{(2)}$ ,  $G^{(3)}$  and  $G^{(4)}$  share the distribution support. However, each distribution  $G^{(k)}$  has completely different bar heights (weights) from another, so HDP does not induce the subject subgroup structure. (b) NDP can achieve the subject subgroup structures, but two distributions in different subgroups do not have the same support, making it hard to match cell types across subgroups. (c) Our prior not only groups subject-specific distributions but also enables cell-type-matching between any two subject subgroups.

### 3 The SCSC Model

We hybridize HDP and NDP into a new nonparametric prior, that succeeds in promoting subject subgroups with shared cell types. The nonparametric prior is constructed by assigning a DP prior to the base measure in the NDP,

$$\begin{aligned}
 G_0 &\sim \text{DP}(\alpha, H), \\
 G^{(j)}(j = 1, \dots, m) &\stackrel{i.i.d.}{\sim} \text{DP}(\nu, \text{DP}(\gamma, G_0)).
 \end{aligned}
 \tag{3.1}$$

Table 1: Comparing the capabilities of the HDP, the NDP and our prior.

Prior	Subject subgroup structures	Shared support
HDP	×	✓
NDP	✓	×
Our prior	✓	✓

On the one hand, since  $G_0$  is drawn from  $DP(\alpha, H)$ , it has a countable support set. This property of  $G_0$  makes the child distributions  $G^{(j)}$ 's share the same support, thus enabling the cell-type-matching across subjects, an important function not favored by NDP. On the other hand, given  $G_0$ , the NDP  $DP(\nu, DP(\gamma, G_0))$  helps to form subgroups for subjects. Therefore, the hierarchical and nested nonparametric prior (3.1) integrates the strengths of HDP and NDP, see Figure 2(c) and Table 1.

Next, we tailor a zero-inflated distribution to the scRNA-seq raw count data and connect the data-modeling part to the proposed nonparametric prior at the final step. We assume that  $Y_{gi}^{(j)}$  is the true read count mapped to gene  $g$  in cell  $i$  for subject  $j$ , but  $Y_{gi}^{(j)}$ 's are only partially observed through the collected data  $X_{gi}^{(j)}$ 's due to the dropout events. Since the probability of happening the dropout relies on the value of  $Y_{gi}^{(j)}$ 's, i.e., the larger the  $Y_{gi}^{(j)}$  the less likely that we observe a zero value, the dropout mechanism is “nonignorable” using the terminology in the field of missing data analysis,

$$X_{gi}^{(j)} = \begin{cases} 0 & \text{with probability } p(Y_{gi}^{(j)}) \\ Y_{gi}^{(j)} & \text{with probability } 1 - p(Y_{gi}^{(j)}) \end{cases}$$

The dropout rate  $p(y)$  is modeled as  $\Phi(\lambda_{g0} + \lambda_{g1} \log_2(y + 1))$  via a Probit link, in which  $\lambda_{g1} < 0$  and  $\Phi$  is the cumulative distribution function of the standard normal distribution. The negative  $\lambda_{g1}$  guarantees the negative correlation between  $y$  and  $p(y)$ , and its dependence on the gene index  $g$  accurately models the biological observations that the dropout rate may be associated with the gene’s features, such as the gene length (Liu et al., 2019), GC contents.

Due to the count nature and over-dispersion of scRNA-seq data, we adopt the Poisson-log-normal (PLN) distribution for the variable  $Y_{gi}^{(j)}$ . The PLN distribution has two parameters  $\eta$  and  $\sigma^2$ , corresponding to the mean and variance of the logarithmic Poisson rate, respectively.

Mathematically,  $Y \sim \text{PLN}(\eta, \sigma^2)$  if and only if  $Y \sim \text{Poi}(e^\theta)$ ,  $\theta \sim \text{N}(\eta, \sigma^2)$ . This equivalence implies that PLN accounts for the over-dispersion (Supplementary Section S1). Note that the cell’s library size is also a factor affecting the magnitude of the read count. We model  $Y_{gi}^{(j)}$  using  $Y_{gi}^{(j)} \sim \text{Poi}(s_i^{(j)} e^{\theta_{gi}^{(j)}})$  and  $\theta_{gi}^{(j)} \sim \text{N}(\eta_{gi}^{(j)}, \sigma_g^2)$ , written as  $Y_{gi}^{(j)} \sim \text{PLN}(s_i^{(j)}, \eta_{gi}^{(j)}, \sigma_g^2)$  for simplicity, where  $s_i^{(j)}$  is a scaling factor to consider cells’ different library sizes. Specifically, if we denote the library size of cell  $i$  in subject  $j$  by  $l_i^{(j)}$ ,  $s_i^{(j)}$  is calculated as  $l_i^{(j)} / \text{median}_i l_i^{(j)}$ , and in practice we let  $l_i^{(j)}$  be  $\sum_{g=1}^G X_{gi}^{(j)}$ . The  $\eta_{gi}^{(j)}$  represents the effects on gene  $g$  caused by cell  $i$  and subject  $j$ , and  $\sigma_g^2$  reflects the variation. We separate cell effects from subject effects and let  $\eta_{gi}^{(j)}$  be the addition of the cell-specific effect  $\mu_{gi}^{(j)}$  and the subject-specific effect  $\beta_g^{(j)}$ .

Combining the dropout mechanism and the PLN distribution for  $Y_{gi}^{(j)}$ ’s gives the zero-inflated PLN (ZIPLN) distribution for the observed data  $X_{gi}^{(j)}$ ’s, which we write as  $X_{gi}^{(j)} \sim \text{ZIPLN}(\lambda_{g0}, \lambda_{g1}, s_i^{(j)}, \mu_{gi}^{(j)} + \beta_g^{(j)}, \sigma_g^2)$ . We notice that  $Y_{gi}^{(j)}$  is from a count-valued distribution with a positive probability at zero, so  $X_{gi}^{(j)} = 0$  results from either  $Y_{gi}^{(j)} = 0$  or  $Y_{gi}^{(j)} > 0$  with a dropout. Hence, dropout events hide themselves among observed zeros and we are not clear which portion of zeros are truly from the dropout, which brings us more difficulty than analyzing the missing data where we know which part is missing.

Lastly, we assign the nonparametric prior (3.1) to the cell-specific effect vector  $\boldsymbol{\mu}_i^{(j)} = (\mu_{1i}^{(j)}, \dots, \mu_{Gi}^{(j)})$ , arriving at the following SCSC (Subject and Cell clustering for Single Cell expression data) model,

$$\begin{aligned}
G_0 &\sim \text{DP}(\alpha, H), \\
G^{(j)}(j = 1, \dots, m) &\stackrel{i.i.d.}{\sim} \text{DP}(\nu, \text{DP}(\gamma, G_0)), \\
\boldsymbol{\mu}_i^{(j)}(i = 1, \dots, n_j) &\stackrel{i.i.d.}{\sim} G^{(j)} \quad \text{for each } j, \\
X_{gi}^{(j)} &\sim \text{ZIPLN}(\lambda_{g0}, \lambda_{g1}, s_i^{(j)}, \mu_{gi}^{(j)} + \beta_g^{(j)}, \sigma_g^2) \quad \text{for each } j, i, \text{ and } g. \quad (3.2)
\end{aligned}$$

We constrain the subject-specific effects  $\beta_g^{(j_1)} = \beta_g^{(j_2)}$  for any  $g$  if  $G^{(j_1)} = G^{(j_2)}$ , as subjects from a subgroup usually exhibit the same characteristic. Moreover, to make the parameters  $\boldsymbol{\mu}$  and  $\boldsymbol{\beta}$  estimable, we let one subject subgroup act as the “reference” group, for example the normal group in biomedical studies, and constrain the subject effects  $\boldsymbol{\beta}^{(j)}$  of the reference group to be zero.

When there are covariates available for cells or subjects, such as batch information for cells or clinical records (e.g., age, gender) for subjects, all of the information can be easily incorporated into the SCSC model by treating them as additive effects on  $\mu_{gi}^{(j)} + \beta_g^{(j)}$  in the ZIPLN distribution. In this way, the SCSC not only detects the heterogeneity among subjects and cells but also estimates how these covariates influence gene expression from the perspective of both subjects and cells.

We acknowledge that other types of count-valued distributions considering the over-dispersion can be used here, for example, the negative-binomial distribution (Risso et al., 2018). SCSC serves as a flexible framework to choose the appropriate sampling distribution depending on the researchers and the problem contexts. We focus on the PLN distribution in the paper mainly for its relative computational convenience.

On the one hand, SCSC has the advantage of simultaneously grouping subjects, clustering cells, and obtaining consistent cell types across subject groups (Figure 2(c)). More importantly, with the benefit of the nonparametric prior (3.1), we do not need to determine the subtype number and the cell type number in advance, both of which can be automatically learned from data. On the other hand, SCSC is carefully designed to account for the count nature, the dropout, the over-dispersion, and the library size of the scRNA-seq data. Therefore, SCSC can be directly applied to the raw count scRNA-seq data without the need of the normalization and avoids the risk of obtaining different results using different normalization strategies.

## 4 Bayesian Inference

The exact posterior sampling for the SCSC model can be carried out by the Polya-urn scheme (Pitman, 1996) that marginalizes all the distributions  $G_0$  and  $G^{(j)}$ 's ( $j \geq 1$ ). However, the marginalization procedure introduces extra dependence among cells and causes the cell-type allocation update for one cell to rely on all other cells. Such a sequential update scheme results in unnecessary and heavy computations. To enhance the posterior sampling efficiency for the SCSC model, we utilize the blocked Gibbs sampler (Ishwaran and James, 2001), where the updates in each parameter block are independent, by taking a truncation strategy (Ishwaran

and James, 2001; Rodriguez et al., 2008)—setting the upper bounds  $L$  for the number of subject subgroups and  $K$  for the cell type number. Moreover, the blocked Gibbs sampler also favors the employment of the parallel computing to further speed up the Bayesian computation. The truncated version of SCSC is

$$\begin{aligned}
G_0 &\sim \text{DP}(\alpha, H), \\
G^{(j)}(j = 1, \dots, m) &\stackrel{i.i.d.}{\sim} \text{DP}_L(\nu, \text{DP}_K(\gamma, G_0)), \\
\boldsymbol{\mu}_i^{(j)}(i = 1, \dots, n_j) &\stackrel{i.i.d.}{\sim} G^{(j)} \quad \text{for each } j, \\
X_{gi}^{(j)} &\sim \text{ZIPLN}(\lambda_{g0}, \lambda_{g1}, s_i^{(j)}, \mu_{gi}^{(j)} + \beta_g^{(j)}, \sigma_g^2) \quad \text{for each } j, i, \text{ and } g. \quad (4.1)
\end{aligned}$$

Using the stick-breaking process metaphor,  $\text{DP}_K(\gamma, G_0)$  indicates we break the unit stick into  $K$  pieces rather than infinite pieces. The following theorem states that the truncation Model (4.1) is an accurate approximation to the original Model (3.2) as long as the truncation numbers  $L$  and  $K$  as well as concentration parameters  $\gamma$  and  $\nu$  are approximately chosen. See the Supplementary Section S2 for the proof, which is based on the Theorem B1 in the NDP paper (Rodriguez et al., 2008).

**Theorem 1.** *Denote the prior distributions of cell effects  $\boldsymbol{\mu}$  from the SCSC model and the truncated SCSC model by  $p^{\infty\infty}(\boldsymbol{\mu})$  and  $p^{KL}(\boldsymbol{\mu})$ , respectively. Based on the priors, we have the marginal distributions  $p^{\infty\infty}(\mathbf{x})$  and  $p^{KL}(\mathbf{x})$  for the observed data  $\mathbf{x}$  by integrating all parameters out. It shows that*

$$\frac{1}{4} \int |p^{KL}(\mathbf{x}) - p^{\infty\infty}(\mathbf{x})| d\mathbf{x} \leq 1 - \left[ 1 - \left( \frac{\nu}{\nu + 1} \right)^{L-1} \right]^m \left[ 1 - \left( \frac{\gamma}{\gamma + 1} \right)^{K-1} \right]^{\sum_{j=1}^m n_j}.$$

If we expand the implicit distributions  $G^{(j)}$ 's in Model (4.1) in terms of subject cluster indicators  $S^{(j)}$ 's and cell type indicators  $C_i^{(j)}$ 's, then Model (4.1) implies a more concrete and interpretable model.

$$\begin{aligned}
\boldsymbol{\xi} &= (\xi_1, \xi_2, \dots, \xi_K) \sim \text{GEM}_K(\alpha), \\
\boldsymbol{\mu}_k &(k = 1, \dots, K) \stackrel{i.i.d.}{\sim} H, \\
\boldsymbol{\pi}_\ell &= (\pi_{1\ell}, \dots, \pi_{K\ell}) (\ell = 1, \dots, L) \stackrel{i.i.d.}{\sim} \text{Dir}(\gamma\xi_1, \gamma\xi_2, \dots, \gamma\xi_K) \\
\boldsymbol{\phi} &= (\phi_1, \phi_2, \dots, \phi_L) \sim \text{GEM}_L(\nu), \\
S^{(j)} &(j = 1, \dots, m) \stackrel{i.i.d.}{\sim} \text{MN}(1; \phi_1, \phi_2, \dots, \phi_L), \\
C_i^{(j)} &(i = 1, \dots, n_j) | S^{(j)} = \ell \stackrel{i.i.d.}{\sim} \text{MN}(1; \pi_{1\ell}, \dots, \pi_{K\ell}) \text{ for each } j, \\
X_{gi}^{(j)} &| S^{(j)} = \ell, C_i^{(j)} = k \sim \text{ZIPLN}(\lambda_{g0}, \lambda_{g1}, s_i^{(j)}, \mu_{gk} + \beta_{g\ell}, \sigma_g^2) \text{ for each } j, i, \text{ and } g.
\end{aligned} \tag{4.2}$$

MN is the multinomial distribution and Dir indicates the Dirichlet distribution.  $\text{GEM}_L(\nu)$  refers to the truncated stick-breaking process in which the stick proportions  $\{\phi'_1, \phi'_2, \dots, \phi'_{L-1}\}$  are i.i.d. from  $\text{Beta}(1, \nu)$  and  $\phi_1 = \phi'_1$ ,  $\phi_\ell = \phi'_\ell \prod_{t=1}^{\ell-1} (1 - \phi'_t)$  for  $2 \leq \ell \leq L-1$ , and  $\phi_L = 1 - \sum_{\ell=1}^{L-1} \phi_\ell$ . The same spirit is for  $\text{GEM}_K(\alpha)$ . Once again, we note that the subgroup one effect vector  $\boldsymbol{\beta}_1$  is fixed at zero for identifiability.

We prove Model (4.2) is equivalent to Model (4.1) in Appendix. From now on, we focus on Model (4.2) to carry out the Bayesian inference.

Next, we specify the priors for unknown parameters in Model (4.2). The priors for concentration parameter  $\alpha$  ( $\alpha > 0$ ) is flat,  $p(\alpha) \propto 1$ . Regarding the baseline distribution  $H$  of cell-type- $k$  effects  $\mu_{gk}$ 's, it is set as the Cartesian product of  $G$  normal distributions  $\text{N}(\eta_\mu, \tau_\mu^2)$ , and we assign priors  $p(\eta_\mu) \propto 1$  and  $p(\tau_\mu^2) \propto \frac{1}{\tau_\mu}$  to  $\eta_\mu$  and  $\tau_\mu^2$ , respectively. Similarly, we assign a normal distribution  $\text{N}(\eta_\beta, \tau_\beta^2)$  to the subtype effect  $\beta_{g\ell}$  and further give  $\eta_\beta$  and  $\tau_\beta^2$  hyper-priors  $p(\eta_\beta) \propto 1$  and  $p(\tau_\beta^2) \propto \frac{1}{\tau_\beta}$  to introduce hierarchy for subject effects, so the information can be borrowed across genes. The variance  $\sigma_g^2$ 's prior distribution is an inverse-gamma distribution  $p(\sigma_g^2) \propto 1/\sigma_g^2$ , and the priors for zero-inflation-related parameters  $\lambda_{g0}$  and  $\lambda_{g1}$  are given by weakly informative priors  $\text{N}(\eta_{\lambda_{g0}}, \tau_{\lambda_{g0}}^2)$  and  $\text{N}(\eta_{\lambda_{g1}}, \tau_{\lambda_{g1}}^2)$ , respectively.

Finally, given the priors and Model (4.2), we utilize the blocked Gibbs sampler (Ishwaran and James, 2001) to carry out the posterior sampling. Since directly sampling from ZIPLN distribution suffers from intractable infinite sum and integral, we augment the auxiliary variables  $\theta_{gi}^{(j)}$  and  $Y_{gi}^{(j)}$  (Tanner and Wong, 1987) specified in Section 3 to make the sampling

for ZIPLN feasible. Accordingly, in each iteration, the sampling scheme proceeds as follows. (“–” means given all other variables)

- 1 The augmented parameter  $\theta_{gi}^{(j)}$  in the PLN distribution is generated from

$$p(\theta_{gi}^{(j)} | -) \propto \exp \left\{ -s_i^{(j)} e^{\theta_{gi}^{(j)}} + Y_{gi}^{(j)} \theta_{gi}^{(j)} - \frac{(\theta_{gi}^{(j)} - \mu_{gk} - \beta_{g\ell})^2}{2\sigma_g^2} \right\},$$

when  $S^{(j)} = \ell$  and  $C_i^{(j)} = k$ .

- 2 Sample the missing variable  $Y_{gi}^{(j)}$  for which its observation  $X_{gi}^{(j)}$  equals zero from

$$p(Y_{gi}^{(j)} | -) \propto \begin{cases} (s_i^{(j)} e^{\theta_{gi}^{(j)}})^{Y_{gi}^{(j)}} / Y_{gi}^{(j)}! \cdot \Phi(\lambda_{g0} + \lambda_{g1} \log_2(Y_{gi}^{(j)} + 1)), & \text{if } Y_{gi}^{(j)} \geq 1 \\ 1, & \text{if } Y_{gi}^{(j)} = 0. \end{cases}$$

- 3 Update the zero-inflation intensity parameters  $\lambda_{g0}$  and  $\lambda_{g1}$  by generating

$$(\lambda_{g0}, \lambda_{g1}) \sim p(\lambda_{g0}, \lambda_{g1} | -) \propto \prod_{(j,i): X_{gi}^{(j)} > 0} \left( 1 - \Phi(\lambda_{g0} + \lambda_{g1} \log_2(Y_{gi}^{(j)} + 1)) \right) \cdot \prod_{(j,i): X_{gi}^{(j)} = 0, Y_{gi}^{(j)} > 0} \Phi \left( \lambda_{g0} + \lambda_{g1} \log_2(Y_{gi}^{(j)} + 1) \right) \cdot N(\lambda_{g0}; \eta_{\lambda_{g0}}, \tau_{\lambda_{g0}}^2) \cdot N(\lambda_{g1}; \eta_{\lambda_{g1}}, \tau_{\lambda_{g1}}^2).$$

The  $N(x; a, b^2)$  represents the density value at  $x$  of a normal distribution with mean  $a$  and standard deviation  $b$ .

- 4 Sample the cell-type  $k$  effect on gene  $g$ ,  $\mu_{gk}$ , from the normal distribution

$$N \left( \frac{\sum_{j=1}^m \sum_{i=1}^{n_j} (\theta_{gi}^{(j)} - \beta_{gS^{(j)}}) I(C_i^{(j)} = k) / \sigma_g^2 + \eta_{\mu} / \tau_{\mu}^2}{\sum_{j=1}^m \sum_{i=1}^{n_j} I(C_i^{(j)} = k) / \sigma_g^2 + 1 / \tau_{\mu}^2}, \frac{1}{\sum_{j=1}^m \sum_{i=1}^{n_j} I(C_i^{(j)} = k) / \sigma_g^2 + 1 / \tau_{\mu}^2} \right),$$

where the  $I(A)$  is an indicator function, being one if  $A$  is true and zero otherwise.

5 Update the hyper-parameters in the cell-type effect prior,

$$p(\eta_\mu|-) \propto \text{N} \left( \sum_{g=1}^G \sum_{k=1}^K \mu_{gk}/GK, \tau_\mu^2/GK \right),$$

$$p(\tau_\mu^2|-) \propto \text{Inv}\Gamma \left( (GK - 1)/2, \sum_{g=1}^G \sum_{k=1}^K (\mu_{gk} - \eta_\mu)^2/2 \right).$$

6 The subgroup  $\ell$  effect on gene  $g$  for  $\ell \geq 2$ ,  $\beta_{g\ell}$ , is sampled from the normal distribution

$$\text{N} \left( \frac{\sum_{j=1}^m \sum_{i=1}^{n_j} (\theta_{gi}^{(j)} - \mu_{gC_i^{(j)}}) I(S^{(j)} = \ell) / \sigma_g^2 + \eta_\beta / \tau_\beta^2}{\sum_{j=1}^m I(S^{(j)} = \ell) n_j / \sigma_g^2 + 1 / \tau_\beta^2}, \frac{1}{\sum_{j=1}^m I(S^{(j)} = \ell) n_j / \sigma_g^2 + 1 / \tau_\beta^2} \right).$$

We notice that subgroup 1 effect,  $\beta_{g1}$ , is restricted to zero across  $1 \leq g \leq G$  for identifying the subgroup and cell-type effects.

7 Update the hyper-parameters in the subgroup effect prior,

$$p(\eta_\beta|-) \propto \text{N} \left( \sum_{g=1}^G \sum_{\ell=2}^L \beta_{g\ell} / G(L-1), \tau_\beta^2 / G(L-1) \right),$$

$$p(\tau_\beta^2|-) \propto \text{Inv}\Gamma \left( (GL - G - 1)/2, \sum_{g=1}^G \sum_{\ell=2}^L (\beta_{g\ell} - \eta_\beta)^2 / 2 \right).$$

8 Update the variance  $\sigma_g^2$  for gene  $g$  by sampling from the inverse-gamma distribution

$$\text{Inv}\Gamma \left( \sum_{j=1}^m n_j / 2, \sum_{j=1}^m \sum_{i=1}^{n_j} (\theta_{gi}^{(j)} - \mu_{gC_i^{(j)}} - \beta_{gS^{(j)}})^2 / 2 \right).$$

9 For each subject  $j$ , update the subtype indicator  $S^{(j)}$  and the cell-type indicators  $C_i^{(j)}$



for cell  $i = 1, \dots, n_j$  from multinomial distributions

$$P(S^{(j)} = \ell | -) \propto \phi_\ell \prod_{i=1}^{n_j} \left[ \sum_{k=1}^K \pi_{k\ell} \prod_{g=1}^G N(\theta_{gi}^{(j)}; \mu_{gk} + \beta_{g\ell}, \sigma_g^2) \right]$$

$$P(C_i^{(j)} = k | S^{(j)} = \ell, -) \propto \pi_{k\ell} \prod_{g=1}^G N(\theta_{gi}^{(j)}; \mu_{gk} + \beta_{g\ell}, \sigma_g^2),$$

$\ell = 1, \dots, L$  and  $k = 1, \dots, K$ .

10 Update the subtype proportion vector  $(\phi_1, \phi_2, \dots, \phi_L)$ . We first sample

$$\phi'_\ell \sim \text{Beta}(1 + m_\ell, \nu + \sum_{j=\ell+1}^L m_j)$$

for  $\ell = 1, \dots, L-1$  and  $\phi'_L := 1$ , where  $m_\ell = \#\{j : S^{(j)} = \ell\}$  is the number of subjects allocated to subgroup  $\ell$ . Subsequently, we let  $\phi_1 = \phi'_1$  and  $\phi_\ell = \phi'_\ell \prod_{i=1}^{\ell-1} (1 - \phi'_i)$  for  $\ell = 2, \dots, L$ .

11 Update the stick-breaking length vector  $(\xi_1, \xi_2, \dots, \xi_K)$ . We first sample

$$p((\xi'_1, \dots, \xi'_{K-1}) | -) \propto \frac{\prod_{k=1}^{K-1} (1 - \xi'_k)^{\alpha-1}}{\prod_{k=1}^K \Gamma^L(\gamma \prod_{i=1}^{k-1} (1 - \xi'_i) \xi'_k)} \prod_{k=1}^K \left( \prod_{\ell=1}^L \pi_{k\ell} \right)^{\gamma \prod_{i=1}^{k-1} (1 - \xi'_i) \xi'_k}.$$

and  $\xi'_K := 1$ . Subsequently, we let  $\xi_1 = \xi'_1$  and  $\xi_k = \prod_{i=1}^{k-1} (1 - \xi'_i) \xi'_k$  for  $k = 2, \dots, K$ .

12 The concentration parameter  $\alpha$  is sampled from the gamma distribution

$$p(\alpha | -) \sim \Gamma \left( K, - \sum_{k=1}^{K-1} \log(1 - \xi'_k) \right),$$

where and  $\xi'_k$ s are the variables generated in the previous iteration.

13 Sample the cell type proportions  $(\pi_{1\ell}, \dots, \pi_{K\ell})$  for each subtype  $\ell$  from the Dirichlet distribution

$$\text{Dir} \left( \sum_{j=1}^m \sum_{i=1}^{n_j} I(S^{(j)} = \ell, C_i^{(j)} = 1) + \gamma \xi_1, \dots, \sum_{j=1}^m \sum_{i=1}^{n_j} I(S^{(j)} = \ell, C_i^{(j)} = K) + \gamma \xi_K \right).$$

For steps 1, 2, 3, and 11 of the blocked Gibbs sampler, they do not correspond to standard distributions, so we design the Metropolis-Hastings (MH) steps to approximate the sampling. The proposal distributions and the calculations of acceptance rates are relegated to Supplementary Section S3. Within each iteration the computational complexity is  $\mathcal{O}(G(K + L) \sum_{j=1}^m n_j)$ , which increases linearly with the gene number, the subject number, and the cell number. Therefore, our MCMC algorithm can scale well on a large volume of scRNA-seq data.

After the burn-in period which is defined as the first half of iterations, we collect the posterior samples from the last half of iterations for statistical inference. For subtype and cell-type indicators,  $S^{(j)}$ 's and  $C_i^{(j)}$ 's, we adopt the mode of the posterior samples to estimate them to keep the integer nature. For the subgroup effects and cell-type-specific effects  $\beta_{gl}$ 's and  $\mu_{gk}$ 's, the posterior mean is used for estimation.

## 5 Results

### 5.1 Simulation

We generated the data following Model (4.2) with three subject subgroups and four cell types. The subject size was chosen as 50, and for each subject we sampled its corresponding cell number from a uniform distribution on integers between 15 and 35. The subject proportion for the three subgroups were 40%, 30%, 30%. For each subject subgroup, we had different cell type proportions  $\boldsymbol{\pi}_\ell$  ( $\ell = 1, 2, 3$ ). Subject subgroup 1 has 20%, 30%, 30%, 20% for cell types from one to four, respectively. If we denote that as  $\boldsymbol{\pi}_1 = (0.2, 0.3, 0.3, 0.2)$ , then we set  $\boldsymbol{\pi}_2 = (0.4, 0.2, 0.3, 0.1)$  for subject subgroup 2 and  $\boldsymbol{\pi}_3 = (0.3, 0.1, 0.3, 0.3)$  for subject subgroup 3. The gene number for each cell was 1,000, and the first 200 genes were treated as marker genes which are differentially expressed in at least two cell types, whereas the remaining genes had the same cell effects across all cell types. With regard to the subject subgroup effects, the subject subgroup 1 effects were fixed at zero. Using the subgroup 1 as the reference, the subgroup 2 had marker genes from 401 to 500, and the subgroup 3 had marker genes from 501 to 600. The generation procedure for the cell type effects and the subgroup effects is

detailed in Supplementary Section S4. The scaling factors were fixed at one. The dropout coefficients  $\lambda_{g0}$  and  $\lambda_{g1}$  were sampled respectively from  $N(3, 0.1^2)$  and  $N(-1, 0.1^2)$ , and the standard deviations  $\sigma_g$ 's were fixed at 0.1.

We then applied our SCSC model to this dataset using the subject subgroup upper bound  $L = 10$ , the cell type number upper bound  $K = 10$ , and  $\gamma = \nu = 0.1$ , which guarantees a very small approximation error  $2.2 \times 10^{-6}$  based on Theorem 1. We carried out  $T = 10,000$  iterations, which cost about 61.68 minutes using 10 CPU cores, and kept the second half of posterior samples for statistical inference. The trace plots of parameters in Supplementary Figure S1 demonstrated the chain had attained convergence by 5,000th iteration. For the number of the occupied subject clusters, its posterior mode is three, and the posterior mode of the occupied cell types is four, both of which are the same as the truth. To measure the clustering accuracy, we used the adjusted random index (ARI) (Hubert and Arabie, 1985), which is bounded above by one, and the larger the ARI, the more accurate the clustering results. It turns out SCSC gave a perfect clustering for subjects as well as cells with both ARIs being one, see Figure 3(e-g). Hence, the SCSC model can automatically and accurately distinguish the underlying heterogeneity for subjects and cells.

By correcting the label-switching, we evaluated the estimates of SCSC for the cell type effects  $\boldsymbol{\mu}$  and the subgroup effects  $\boldsymbol{\beta}$ . The Figure 3(a-d) shows the comparison between the true parameter values and the estimates, indicating that the SCSC model estimated the two types of effects well. With the available posterior samples of  $\boldsymbol{\mu}$  and  $\boldsymbol{\beta}$ , we further detected the DE genes across cell types or subject subgroups using Bayesian credible intervals. For example, if we test whether gene  $g$  is DE between cell type 1 and cell type  $k$  ( $k \geq 2$ ), we constructed the 99% credible interval for the difference  $\mu_{gk} - \mu_{g1}$  using the posterior samples. If zero is not in this credible interval, then we treat the gene as DE. Otherwise, the gene is non-DE. Although we conducted multiple hypothesis testings, we do not need to implement multiple comparison adjustments as  $\boldsymbol{\mu}$  and  $\boldsymbol{\beta}$  were modeled in a hierarchical Bayesian fashion (Gelman et al., 2012). The similar procedure was applied to detecting DE genes across subject subgroups. It turns out that SCSC correctly detected most of DE genes with high power and small false positive rates as shown in Supplementary Table S1.

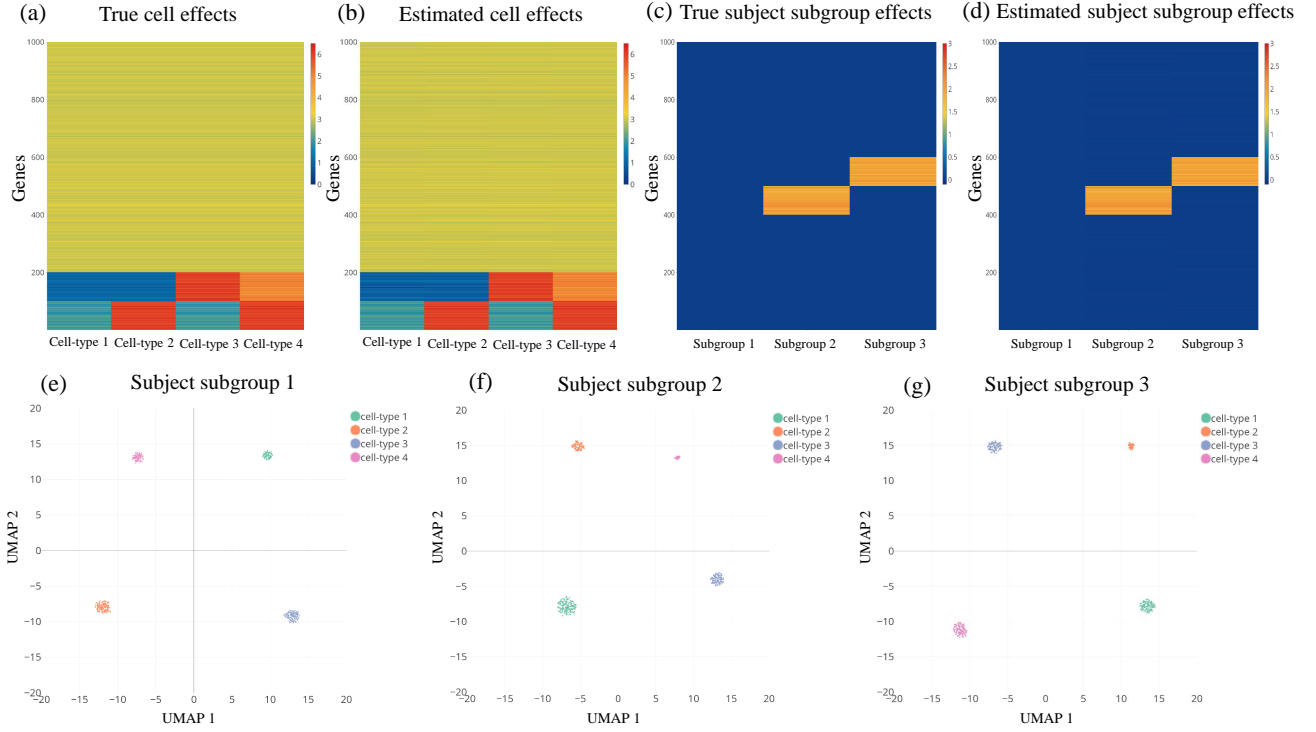


Figure 3: The performance of the SCSC model in the simulation study. (a) The heatmap of the true cell effects  $\mu_{gk}$ 's and (b) the heatmap of cell effect estimations. In both (a) and (b), one row is one gene and each column represents one cell type. (c) The heatmap of the true subject subgroup effects and (d) the heatmap of subject subgroup effect estimations. In both (c) and (d), one row is one gene and each column represents one subject subgroup. (e-g) The scatter plots of the cells after the dimension reduction with two UMAP components in subject subgroup 1, 2, and 3, respectively.

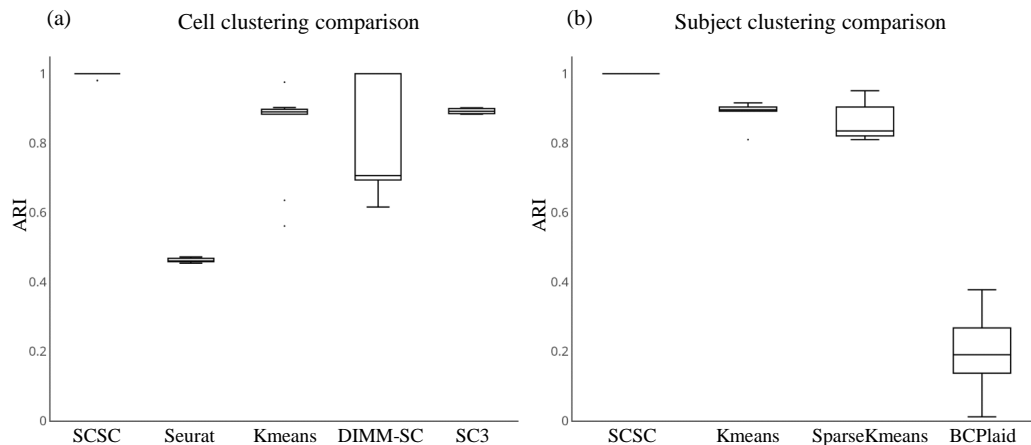


Figure 4: The clustering performances of the SCSC model as well as competing methods in the cell clustering and the subject clustering settings based on ten realizations. (a) The ARI box plots for SCSC and other cell clustering approaches. (b) The ARI box plots for SCSC and other subject clustering approaches. The implementation details of the competing methods are provided in the Supplementary Section S5.

Since there is no statistical approach to simultaneously cluster subjects and cells, we compared SCSC against some popular cell clustering approaches and subject clustering approaches, respectively. For the cell clustering approaches Kmeans (MacQueen et al., 1967), SC3 (Kiselev et al., 2017), DIMM-SC (Sun et al., 2017), Seurat (Butler et al., 2018; Stuart et al., 2018), we stacked the expression matrices for all subjects by row and used this large expression matrix as the input. With regard to the subject clustering approaches Kmeans (MacQueen et al., 1967), SparseKmeans (Witten and Tibshirani, 2010) and BCPlaid (Turner et al., 2005), we calculated the row means of its corresponding expression matrix (logarithm transformed) for each subject and combined all row means to form a gene by subject aggregated expression matrix. The Figure 4 displays the boxplots for ARI values of all methods under the cell clustering setting and the subject clustering setting based on ten realizations. Overall, SCSC performed the best in both cell clustering and subject clustering. When clustering cells, SCSC borrows information across multiple subjects and considers the subject differences. When grouping subjects, SCSC takes advantage of the cell information of each subject to discover the subtle difference. Thanks to the two-way information-sharing strategy, SCSC outperforms competing methods in both cell clustering and subject grouping.

## 5.2 Real Application

Sarkar et al. (2019) collected scRNA-seq datasets from 7585 induced pluripotent stem cells (iPSCs) in a total of 54 Yoruba subjects in Nigeria. The datasets are publicly available with the accession code GSE118723 in GEO (Edgar et al., 2002). Although the purpose of the study (Sarkar et al., 2019) is to detect variance QTLs, we can use the same dataset to mine out other interesting information, such as the cell and subject heterogeneity presented here. At the subject level, Yoruba is one of Nigeria’s largest ethnic groups, and Yoruba people in the same lineage are more likely to have similar social habits, political preferences (Schwab, 1955) or to suffer from the same genetic diseases (Olaitan et al., 2014). Therefore, analyzing the heterogeneity of the Yoruba people can help clarify their family relationships or even find Yoruba sub-races. At the cell level, the iPSCs are reprogrammed from the somatic cells in adult tissues and have the ability to differentiate into many cell types, so they can be potentially used to make personalized treatments for patients. The iPSCs derived from different somatic cell types may demonstrate heterogeneous differentiation abilities (Kim et al., 2011). Our aim is to apply SCSC to the dataset to distinguish Yoruba individuals and separate the iPSC heterogeneity at the same time.

Our analysis focused on scRNA-seq counts from batch 6 in their study, which includes 20 subjects and 1152 cells. In the preprocessing procedure, we filtered out cells with the zero proportion more than 80% and genes with the zero proportion more than 30%, and further removed subjects having less than 5 cells, resulting in a scRNA-seq dataset with 14 subjects, 1028 cells, and 4178 genes. The cell numbers of the selected 14 subjects range from 29 to 129. During the analysis, the scaling factors for each cells were computed to adjust the effects of library sizes.

We next carried out the SCSC model with the subject subgroup upper bound 10 and the cell type upper bound 10. The blocked Gibbs sampler proceeded 10,000 iterations with the first half as the burn-in period, and it took about 4.63 hours using 10 CPU cores. The trace plots in Supplementary Figure S2 showed that the chains had attained convergence during burn-in. Two Yoruba subgroups and two iPSC types were identified. Yoruba subgroup 1

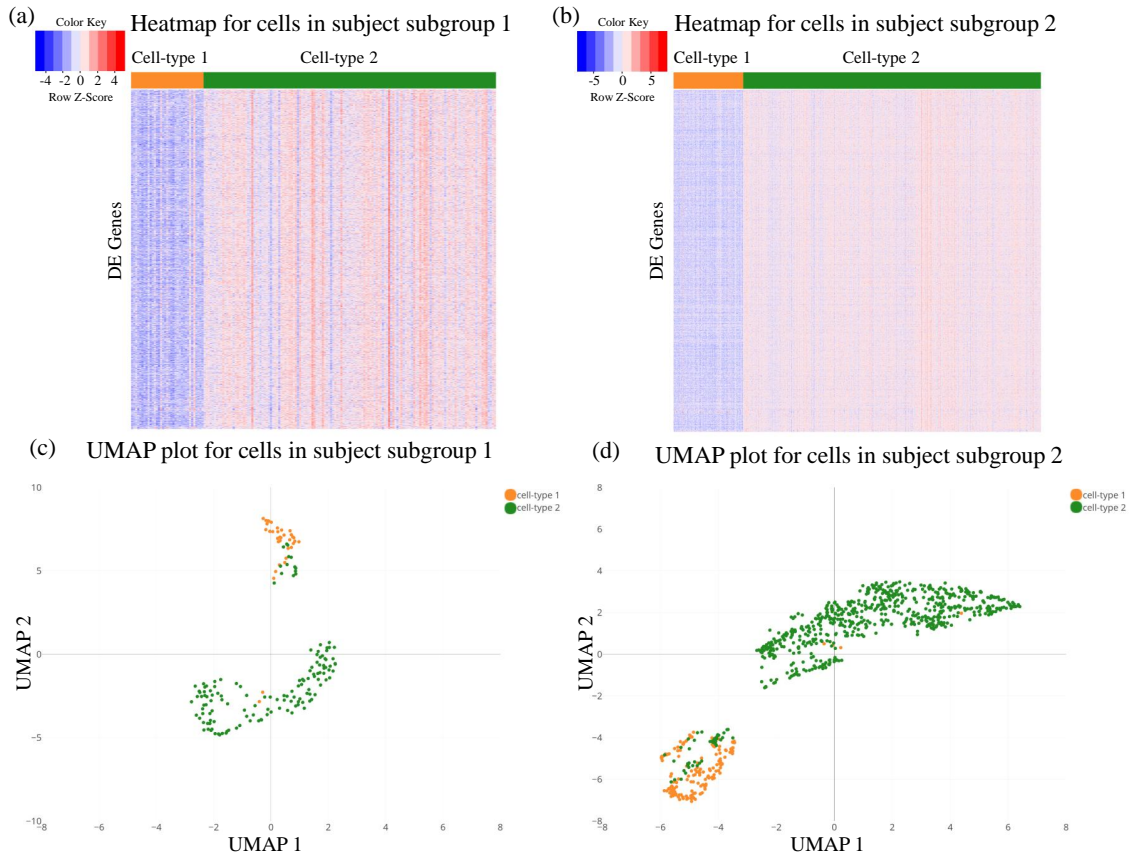


Figure 5: The performance of SCSC on the Yoruba iPSC scRNA-seq data. (a) The heatmap for the logarithm-transformed and row-scaled gene expression values of cells in subject subgroup 1, where each row corresponds to one detected DE gene between the two cell types and each column represents a cell. There are 2662 DE genes, 35 type 1 cells, and 141 type 2 cells. Cells under the same color are from the same cell type. (b) The heatmap for logarithm-transformed and row-scaled gene expression values of cells in subject subgroup 2. Rows and columns have the same meaning as those of the previous heatmap. There are 2662 DE genes, 162 type 1 cells, and 690 type 2 cells. (c-f) The scatter plots by projecting cells in subject subgroups 1 and 2 to a two dimensional space using UMAP. Cells are colored by the estimated cell types: cell type 1 (orange), cell type 2 (green).

contains two subjects and have cellular compositions 19.89%, 80.11% for cell types 1 and 2. Subgroup 2 Yoruba contains twelve subjects with cell type compositions 19.01%, 80.99%. The Figure 5(a) and 5(b) showed the heatmaps for logarithm transformed and row scaled expression values in Yoruba subgroups 1 and 2, respectively. We observed obviously differential expression patterns between cell types 1 and 2 on detected cell type DE genes, indicating there indeed exists heterogeneity among iPSCs. Besides the cellular compositions, the estimated effects of the Yoruba subgroups also demonstrated the heterogeneity of the Yoruba individuals (Supplementary Figure 3). The cells in each Yoruba subgroup were projected into a two-dimensional UMAP scatter plot using the R package `umap` (Konopka, 2019). Figure 5(c-d) show a clear cell pattern in Yoruba subgroups 1-2: cells of type 1 (orange) and type 2 (green) are well-separated.

To validate the clustering results, we conducted the gene set enrichment analysis (Subramanian et al., 2005) for detected marker genes based on the KEGG database. The marker genes for Yoruba subgroups or iPSC types were called if they are DE in at least one subgroup or cell type, respectively. We identified 602 intrinsic genes between the Yoruba subgroups and found 40 significant pathways with  $q$ -value  $< 0.05$  (Supplementary Table S2), where three pathways `KEGG_PARKINSONS_DISEASE`, `KEGG_HUNTINGTONS_DISEASE`, and `KEGG_ALZHEIMERS_DISEASE` are all related to neurodegenerative disorders. Previous studies (Myers, 2004; Bertram and Tanzi, 2008; Shulman et al., 2011) have presented that the three diseases are likely caused by inheritable gene defects and thus can be inherited from one generation to the next. The observations reflect that SCSC separated the Yoruba subjects possibly in terms of the lineage. In addition, we detected 2662 DE genes across the cell types and identified 74 significant pathways (Supplementary Table S3 and S4) including `KEGG_RIBOSOME`, `KEGG_P53_SIGNALING_PATHWAY`, `KEGG_WNT_SIGNALING_PATHWAY`, `KEGG_NOTCH_SIGNALING_PATHWAY`, and `KEGG_MTOR_SIGNALING_PATHWAY`. Since the ribosomes play a critical role in the translation process from mRNAs to proteins, the two iPSC types may have differences in genes related to ribosome generation. In addition, the four signaling pathways may regulate the pluripotency of induced stem cells (Ye et al., 2012; Kate et al., 2014; Meng et al., 2018). These



findings indicate the validity of the SCSC in discovering subject and cell heterogeneity.

## 6 Conclusion

We develop a nonparametric Bayesian model SCSC to simultaneously discover subject and cell heterogeneity in a two-level clustering way. SCSC has the flexibility of learning the subject subgroup number or the cell type number by data without a prespecification. Different from the priors HDP or NDP, we proposed the nonparametric Bayesian prior of SCSC to induce group structures in subjects, cluster cells in each subject, and match cell types across subjects. The ZIPLN distribution employed in SCSC directly models the count nature, over-dispersion, and dropouts of the scRNA-seq data. Owing to the two features, the SCSC model achieves the subject-level and cell-level clustering on the multi-subject scRNA-seq data. When clustering subjects, SCSC takes advantage of the cell-resolution differences; and when clustering cells, SCSC borrows information across multiple subjects. The two-way information-sharing strategy enables SCSC to obtain more accurate clustering results than competing methods in the domain of either subject clustering using bulk expression data or cell clustering based on scRNA-seq data.

To the best of our knowledge, SCSC is the first unified approach to addressing the two-level clustering for scRNA-seq data. Especially, SCSC bridges the methodology gap between the subject clustering based on aggregated gene expression data and the scRNA-seq cell clustering. The framework in SCSC can be further adapted to any situations where the observed data are sparse, count-valued and the two-level clustering are of interest. For example, in the text mining context, a topic can be treated as a subject, a document represents a cell, and the word dictionary corresponds to the gene set. The word frequency data are also count and highly sparse. Thus, SCSC can be applied to finding the topic groups as well as document clusters. With the continuous progress of the sequencing technology, the single cell RNA sequencing will be affordable and available for more and more people. Therefore, we envision that the SCSC model can be a useful method to facilitate the development of the personalized treatment in the time of single cell genomics.

# Appendix

We prove that Model (4.2) is equivalent to Model (4.1).

*Proof.* In Model (4.1), we first focus on the first three lines,

$$\left\{ \begin{array}{l} G_0 \sim \text{DP}(\alpha, H) \\ G^{(j)}|G_0 \sim \text{DP}_L(\nu, \text{DP}_K(\gamma, G_0)) \\ \boldsymbol{\mu}_i^{(j)}|G^{(j)} \sim G^{(j)} \end{array} \right\} \iff (*) \left\{ \begin{array}{l} G_0 \sim \text{DP}(\alpha, H) \\ G_\ell^*|G_0 \sim \text{DP}_K(\gamma, G_0) \text{ for } 1 \leq \ell \leq L \\ \boldsymbol{\phi} = (\phi_1, \phi_2, \dots, \phi_L) \sim \text{GEM}_L(\nu) \\ G^{(j)}|G_\ell^*, \boldsymbol{\phi} \sim \sum_{\ell=1}^L \phi_\ell \delta_{G_\ell^*} \\ \boldsymbol{\mu}_i^{(j)}|G^{(j)} \sim G^{(j)}. \end{array} \right.$$

Note that  $G_0 \sim \text{DP}(\alpha, H)$  and  $G_\ell^*|G_0 \sim \text{DP}(\gamma, G_0)$  are equivalent to  $\boldsymbol{\rho} = (\rho_1, \rho_2, \dots) \sim \text{GEM}(\alpha)$ ,  $\boldsymbol{\mu}_k \sim H$ ,  $\boldsymbol{\pi}'_\ell = (\pi'_{1\ell}, \pi'_{2\ell}, \dots)|\boldsymbol{\rho} \sim \text{DP}(\gamma, \boldsymbol{\rho})$  and  $G_\ell^{*\prime} = \sum_{k=1}^\infty \pi'_{k\ell} \delta_{\boldsymbol{\mu}_k}$  according to the results from HDP (Teh et al., 2006). Subsequently, when there is a truncation  $K$  on the distribution  $G_\ell^{*\prime} = \sum_{k=1}^\infty \pi'_{k\ell} \delta_{\boldsymbol{\mu}_k}$ , we have  $G_\ell^* = \sum_{k=1}^K \pi_{k\ell} \delta_{\boldsymbol{\mu}_k}$ , where  $\pi_{k\ell} = \pi'_{k\ell}$  for  $1 \leq k \leq K-1$  and  $\pi_{K\ell} = \sum_{i=K}^\infty \pi'_{i\ell}$ . Therefore, the first two lines of the expression (\*) are

$$\left\{ \begin{array}{l} G_0 \sim \text{DP}(\alpha, H) \\ G_\ell^* | G_0 \sim \text{DP}_K(\gamma, G_0) \end{array} \right\} \iff \left\{ \begin{array}{l} \boldsymbol{\rho} = (\rho_1, \rho_2, \dots) \sim \text{GEM}(\alpha) \\ \boldsymbol{\mu}_k \sim H \\ \boldsymbol{\pi}_\ell = (\pi_{1,\ell}, \dots, \pi_{K-1,\ell}, \pi_{K,\ell}) | \boldsymbol{\rho} \\ \quad \sim \text{Dir}(\gamma \rho_1, \dots, \gamma \rho_{K-1}, \gamma \sum_{i=K}^{\infty} \rho_i) \\ G_\ell^* | \boldsymbol{\pi}_\ell, \boldsymbol{\mu}_k = \sum_{k=1}^K \pi_{k\ell} \delta_{\boldsymbol{\mu}_k} \end{array} \right. \\
\iff \left\{ \begin{array}{l} \boldsymbol{\xi} := (\xi_1 = \rho_1, \dots, \xi_{K-1} = \rho_{K-1}, \xi_K = \sum_{i=K}^{\infty} \rho_i) \\ \quad \sim \text{GEM}_K(\alpha) \\ \boldsymbol{\mu}_k \sim H \\ \boldsymbol{\pi}_\ell | \boldsymbol{\xi} \sim \text{Dir}(\gamma \xi_1, \dots, \gamma \xi_K) \\ G_\ell^* | \boldsymbol{\pi}_\ell, \boldsymbol{\mu}_k \sim \sum_{k=1}^K \pi_{k\ell} \delta_{\boldsymbol{\mu}_k}. \end{array} \right.$$

The second equivalence holds because for any  $\boldsymbol{\xi} \sim \text{GEM}_K(\alpha)$  we can find a  $\boldsymbol{\rho}$  following  $\text{GEM}(\alpha)$  by letting  $\rho_k = \xi_k$  for  $1 \leq k \leq K-1$ ,  $\rho_K = (1 - \sum_{i=1}^{K-1} \rho_i) \cdot \rho'_K$ , and  $\rho_k = (1 - \sum_{i=1}^{K-1} \rho_i) \cdot \prod_{i=K}^{k-1} (1 - \rho'_i) \cdot \rho'_k$  for  $k \geq K+1$ , where  $\rho'_i \sim \text{Beta}(1, \alpha)$  ( $i \geq K$ ); and on the opposite direction, for any  $\boldsymbol{\rho} \sim \text{GEM}(\alpha)$ ,  $\boldsymbol{\xi}$  follows  $\text{GEM}_K(\alpha)$  through the construction above. Next, we plug the result above into the expression (\*), leading to

$$\left\{ \begin{array}{l} G_0 \sim \text{DP}(\alpha, H) \\ G^{(j)} | G_0 \sim \text{DP}_L(\nu, \text{DP}_K(\gamma, G_0)) \\ \boldsymbol{\mu}_i^{(j)} | G^{(j)} \sim G^{(j)} \end{array} \right\} \iff \left\{ \begin{array}{l} \boldsymbol{\xi} \sim \text{GEM}_K(\alpha) \\ \boldsymbol{\mu}_k \sim H \\ \boldsymbol{\pi}_\ell | \boldsymbol{\xi} \sim \text{Dir}(\gamma \xi_1, \dots, \gamma \xi_K) \\ G_\ell^* | \boldsymbol{\pi}_\ell, \boldsymbol{\mu}_k = \sum_{k=1}^K \pi_{k\ell} \delta_{\boldsymbol{\mu}_k} \\ \boldsymbol{\phi} = (\phi_1, \phi_2, \dots, \phi_L) \sim \text{GEM}_L(\nu) \\ G^{(j)} | G_\ell^*, \boldsymbol{\phi} \sim \sum_{\ell=1}^L \phi_\ell \delta_{G_\ell^*} \\ \boldsymbol{\mu}_i^{(j)} | G^{(j)} \sim G^{(j)}. \end{array} \right.$$

Considering  $S^{(j)}$ ,  $C_i^{(j)}$ , and the distribution for scRNA-seq data, it follows that

$$\left\{ \begin{array}{l} G_0 \sim \text{DP}(\alpha, H) \\ G^{(j)} | G_0 \sim \text{DP}_L(\nu, \text{DP}_K(\gamma, G_0)) \\ \boldsymbol{\mu}_i^{(j)} | G^{(j)} \sim G^{(j)} \\ X_{gi}^{(j)} | \boldsymbol{\mu}_i^{(j)} \sim \\ \quad \text{ZIPLN}(\lambda_{g0}, \lambda_{g1}, s_i^{(j)}, \mu_{gi}^{(j)} + \beta_g^{(j)}, \sigma_g^2) \end{array} \right. \iff \left\{ \begin{array}{l} \boldsymbol{\xi} \sim \text{GEM}_K(\alpha) \\ \boldsymbol{\mu}_k \sim H \\ \boldsymbol{\pi}_\ell \sim \text{Dir}(\gamma \boldsymbol{\xi}_1, \dots, \gamma \boldsymbol{\xi}_K) \\ \boldsymbol{\phi} = (\phi_1, \phi_2, \dots, \phi_L) \sim \text{GEM}_L(\nu) \\ S^{(j)} \sim \text{MN}(1; \phi_1, \phi_2, \dots, \phi_L) \\ C_i^{(j)} | S^{(j)} = \ell \sim \text{MN}(1; \pi_{1\ell}, \dots, \pi_{K\ell}) \\ X_{gi}^{(j)} | S^{(j)} = \ell, C_i^{(j)} = k \sim \\ \quad \text{ZIPLN}(\lambda_{g0}, \lambda_{g1}, s_i^{(j)}, \mu_{gk} + \beta_{g\ell}, \sigma_g^2). \end{array} \right.$$

□

## References

- Becht, E., L. McInnes, J. Healy, C.-A. Dutertre, I. W. Kwok, L. G. Ng, F. Ginhoux, and E. W. Newell (2019). Dimensionality reduction for visualizing single-cell data using UMAP. *Nature Biotechnology* 37(1), 38.
- Bertram, L. and R. E. Tanzi (2008). Thirty years of Alzheimer’s disease genetics: the implications of systematic meta-analyses. *Nature Reviews Neuroscience* 9(10), 768.
- Buettner, F., K. N. Natarajan, F. P. Casale, V. Proserpio, A. Scialdone, F. J. Theis, S. A. Teichmann, J. C. Marioni, and O. Stegle (2015). Computational analysis of cell-to-cell heterogeneity in single-cell RNA-sequencing data reveals hidden subpopulations of cells. *Nature Biotechnology* 33(2), 155–160.
- Busch, S. E., M. L. Hanke, J. Kargl, H. E. Metz, D. Macpherson, and A. M. Houghton (2016).

- Lung cancer subtypes generate unique immune responses. *Journal of Immunology* 197(11), 4493–4503.
- Butler, A., P. Hoffman, P. Smibert, E. Papalexi, and R. Satija (2018). Integrating single-cell transcriptomic data across different conditions, technologies, and species. *Nature Biotechnology* 36(5), 411.
- Cheng, Y. and G. M. Church (2000). Biclustering of expression data. 8, 93–103.
- Der Maaten, L. V. and G. E. Hinton (2008). Visualizing data using t-SNE. *Journal of Machine Learning Research* 9, 2579–2605.
- Edgar, R., M. Domrachev, and A. E. Lash (2002). Gene Expression Omnibus: NCBI gene expression and hybridization array data repository. *Nucleic Acids Research* 30(1), 207–210.
- Ferguson, T. S. (1973). A Bayesian analysis of some nonparametric problems. *Annals of Statistics* 1(2), 209–230.
- Gelman, A., J. Hill, and M. Yajima (2012). Why we (usually) don’t have to worry about multiple comparisons. *Journal of Research on Educational Effectiveness* 5(2), 189–211.
- Huang, M., J. Wang, E. A. Torre, H. Dueck, S. M. Shaffer, R. Bonasio, J. I. Murray, A. Raj, M. Li, and N. R. Zhang (2018). SAVER: gene expression recovery for single-cell RNA sequencing. *Nature Methods* 15(7), 1.
- Hubert, L. and P. Arabie (1985). Comparing partitions. *Journal of Classification* 2(1), 193–218.
- Huo, Z., Y. Ding, S. Liu, S. Oesterreich, and G. Tseng (2016). Meta-analytic framework for sparse K-means to identify disease subtypes in multiple transcriptomic studies. *Journal of the American Statistical Association* 111(513), 27–42.
- Ishwaran, H. and L. F. James (2001). Gibbs sampling methods for stick-breaking priors. *Journal of the American Statistical Association* 96(453), 161–173.

- Jia, C., Y. Hu, D. Kelly, J. Kim, M. Li, and N. R. Zhang (2017). Accounting for technical noise in differential expression analysis of single-cell RNA sequencing data. *Nucleic Acids Research* 45(19), 10978–10988.
- Kate, Hawkins, and Tristan (2014). Cell signalling pathways underlying induced pluripotent stem cell reprogramming. *World Journal of Stem Cells* 6(5), 620.
- Kim, K., R. Zhao, A. Doi, K. Ng, J. Unternaehrer, P. Cahan, H. Hongguang, Y. Loh, M. J. Aryee, M. W. Lensch, et al. (2011). Donor cell type can influence the epigenome and differentiation potential of human induced pluripotent stem cells. *Nature Biotechnology* 29(12), 1117–1119.
- Kiselev, V. Y., K. Kirschner, M. T. Schaub, T. Andrews, A. Yiu, T. Chandra, K. N. Natarajan, W. Reik, M. Barahona, and A. R. Green (2017). SC3: consensus clustering of single-cell RNA-seq data. *Nature Methods* 14(5), 483–486.
- Konopka, T. (2019). *UMAP: uniform manifold approximation and projection*. R package version 0.2.1.0.
- Lin, P., M. Troup, and J. W. K. Ho (2017). CIDR: Ultrafast and accurate clustering through imputation for single-cell RNA-seq data. *Genome Biology* 18(1), 59.
- Liu, Y., L. J. Warren, and H. Zhao (2019). A hierarchical Bayesian model for single-cell clustering using RNA-sequencing data. *The Annals of Applied Statistics*.
- Lopez, R., J. Regier, M. B. Cole, M. I. Jordan, and N. Yosef (2018). Deep generative modeling for single-cell transcriptomics. *Nature Methods* 15(12), 1053–1058.
- Luo, X. and Y. Wei (2019). Batch effects correction with unknown subtypes. *Journal of the American Statistical Association* 114(526), 581–594.
- MacQueen, J. et al. (1967). Some methods for classification and analysis of multivariate observations. In *Proceedings of the fifth Berkeley symposium on mathematical statistics and probability*, Volume 1, pp. 281–297. Oakland, CA, USA.

- Makki, J. (2015). Diversity of breast carcinoma: Histological subtypes and clinical relevance. *Clinical Medicine Insights Pathology* 8(8), 23–31.
- Meng, D., A. R. Frank, and J. L. Jewell (2018). mTOR signaling in stem and progenitor cells. *Development* 145(1), dev152595.
- Myers, R. H. (2004). Huntington’s disease genetics. *NeuroRx* 1(2), 255–262.
- Ntranos, V., G. M. Kamath, J. Zhang, L. Pachter, and D. Tse (2016). Fast and accurate single-cell RNA-seq analysis by clustering of transcript-compatibility counts. *Genome Biology* 17(1), 112.
- Olaitan, P. B., V. Odesina, S. A. Ademola, S. O. Fadiora, O. M. Oluwatosin, and E. J. Reichenberger (2014). Recruitment of Yoruba families from Nigeria for genetic research: experience from a multisite keloid study. *BMC Medical Ethics* 15(1), 65–65.
- Pan, W. and X. Shen (2007). Penalized model-based clustering with application to variable selection. *Journal of Machine Learning Research* 8(May), 1145–1164.
- Pierson, E. and C. Yau (2015). ZIFA: Dimensionality reduction for zero-inflated single-cell gene expression analysis. *Genome Biology* 16(1), 241–241.
- Pitman, J. (1996). Some developments of the Blackwell-Macqueen urn scheme. *Lecture Notes-Monograph Series* 30, 245–267.
- Prabhakaran, S., E. Azizi, A. Carr, and D. Pe’er (2016). Dirichlet process mixture model for correcting technical variation in single-cell gene expression data. In *International Conference on Machine Learning*.
- Prelic, A., S. Bleuler, P. Zimmermann, A. Wille, P. Buhlmann, W. Gruissem, L. Hennig, L. Thiele, and E. Zitzler (2006). A systematic comparison and evaluation of biclustering methods for gene expression data. *Bioinformatics* 22(9), 1122–1129.

- Risso, D., F. Perraudou, S. Gribkova, S. Dudoit, and J. Vert (2018). A general and flexible method for signal extraction from single-cell RNA-seq data. *Nature Communications* 9(1), 284.
- Rodriguez, A., D. B. Dunson, and A. E. Gelfand (2008). The nested dirichlet process. *Journal of the American Statistical Association* 103(483), 1131–1154.
- Rozenblatt-Rosen, O., M. J. Stubbington, A. Regev, and S. A. Teichmann (2017). The Human Cell Atlas: from vision to reality. *Nature News* 550(7677), 451.
- Sarkar, A. K., P.-Y. Tung, J. D. Blischak, J. E. Burnett, Y. I. Li, M. Stephens, and Y. Gilad (2019). Discovery and characterization of variance QTLs in human induced pluripotent stem cells. *PLoS genetics* 15(4), e1008045.
- Schwab, W. B. (1955). Kinship and lineage among the Yoruba. *Africa* 25(04), 352–374.
- Sethuraman, J. (1991). A constructive definition of dirichlet priors. *Statistics Sinica* 4(2), 639–650.
- Shulman, J. M., P. L. De Jager, and M. B. Feany (2011). Parkinson’s disease: genetics and pathogenesis. *Annual Review of Pathology: Mechanisms of Disease* 6, 193–222.
- Sinha, D., A. Kumar, H. Kumar, S. Bandyopadhyay, and D. Sengupta (2018). dropClust: efficient clustering of ultra-large scRNA-seq data. *Nucleic Acids Research* 46(6).
- Song, F., G. M. Chan, and Y. Wei (2019). Flexible experimental designs for valid single-cell RNA-sequencing experiments allowing batch effects correction. *bioRxiv*, 533372.
- Stuart, T., A. Butler, P. Hoffman, C. Hafemeister, E. Papalexi, W. M. Mauck, M. Stoeckius, P. Smibert, and R. Satija (2018). Comprehensive integration of single cell data. *bioRxiv*, 460147.
- Subramanian, A., P. Tamayo, V. K. Mootha, S. Mukherjee, B. L. Ebert, M. A. Gillette, A. G. Paulovich, S. L. Pomeroy, T. R. Golub, E. S. Lander, et al. (2005). Gene set enrichment analysis: A knowledge-based approach for interpreting genome-wide expression profiles.



*Proceedings of the National Academy of Sciences of the United States of America* 102(43), 15545–15550.

Sun, Z., T. Wang, K. Deng, W. XF, R. Lafyatis, Y. Ding, M. Hu, and W. Chen (2017). DIMM-SC: a Dirichlet mixture model for clustering droplet-based single cell transcriptomic data. *Bioinformatics* 34(1).

Tanner, M. and W. H. Wong (1987). The calculation of posterior distributions by data augmentation. *Journal of the American Statistical Association* 82(398), 528–540.

Teh, Y. W., M. I. Jordan, M. J. Beal, and D. M. Blei (2006). Hierarchical dirichlet processes. *Journal of the American Statistical Association* 101(476), 1566–1581.

Turner, H., T. C. Bailey, and W. J. Krzanowski (2005). Improved biclustering of microarray data demonstrated through systematic performance tests. *Computational Statistics & Data Analysis* 48(2), 235–254.

Van Dijk, D., J. Nainys, R. Sharma, P. Kathail, A. Carr, K. R. Moon, L. Mazutis, G. Wolf, S. Krishnaswamy, and D. Peer (2017). MAGIC: A diffusion-based imputation method reveals gene-gene interactions in single-cell RNA-sequencing data. *bioRxiv*, 111591.

Wang, S. and J. Zhu (2008). Variable selection for model-based high-dimensional clustering and its application to microarray data. *Biometrics* 64(2), 440–448.

Witten, D. M. and R. Tibshirani (2010). A framework for feature selection in clustering. *Journal of the American Statistical Association* 105(490), 713–726.

Yau, C. et al. (2016). pcaReduce: hierarchical clustering of single cell transcriptional profiles. *BMC bioinformatics* 17(1), 140.

Ye, D., G. Wang, Y. Liu, W. Huang, M. Wu, S. Zhu, W. Jia, A.-M. Deng, H. Liu, and J. Kang (2012). MiR-138 promotes induced pluripotent stem cell generation through the regulation of the p53 signaling. *Stem Cells* 30(8), 1645–1654.

Zhang, L. and S. Zhang (2018). PBLR: an accurate single cell RNA-seq data imputation tool considering cell heterogeneity and prior expression level of dropouts. *bioRxiv*.